Identification of transient heat sources using the reciprocity gap

Nicolas Auffray, Marc Bonnet, Stéphane Pagano

Identification of transient heat sources using the reciprocity gap

Nicolas Auffray[a,2], Marc Bonnet[a,1,*], Stéphane Pagano[b,3]

[a]*Laboratoire de Mécanique des Solides, CNRS, École Polytechnique, Palaiseau, France.*
[b]*Laboratoire de Mécanique et Génie Civil (LMGC), CNRS, Université Montpellier 2, Montpellier, France*

Abstract

The deformation of solid materials is nearly always accompanied with temperature variations, induced by intrinsic dissipation and thermomechanical coupling. Heat sources give precious information on the thermomechanical behavior of materials. They can be indirectly observed from thermal measurements on the specimen boundary, obtained e.g. via infrared thermography. To solve the inverse problem of identifying heat sources from such observations, a non-iterative algebraical method based on the Reciprocity Gap Method is proposed. This approach, used elsewhere mainly for time-independent identification, is applied here to transient measurements. Under appropriate modelling assumptions the number of heat sources, their spatial locations and energies are retrieved, as demonstrated on numerical experiments where the robustness of the method to measurement noise is also studied.

Keywords: Inverse problem, Heat equation, Source identification, Reciprocity Gap, Non-iterative method.

1. Introduction

1.1. Physical motivation

The deformation of solid materials is nearly always accompanied with temperature variations. These variations, induced by intrinsic dissipation of energy and thermomechanical coupling, are governed by the heat diffusion equation stemming from the first and second laws of thermodynamics:

$$\rho C \partial_t \vartheta - k \Delta \vartheta = f, \tag{1}$$

where ϑ is the temperature, ρ, C, k are respectively the mass density, the specific heat capacity and the thermal conductivity (which in this article are assumed to be homogeneous and, for the conductivity, isotropic). The thermomechanical source term has the form $f = \mathcal{D} + \mathcal{T}$, where $\mathcal{D}$ is the intrinsic dissipation (caused by e.g. plasticity) and $\mathcal{T} := \rho \vartheta \partial^2_{\vartheta \alpha_j} \psi \cdot \dot{\alpha}_j$ (where ψ is the free energy density and α_j are the internal variables) is associated to thermomechanical couplings [8]. In (1) and thereafter, the shorthand ∂_X denotes the partial derivative w.r.t. a variable X.

Quantitative evaluation of such sources therefore provides important information on the thermomechanical behavior of the material. Infrared thermography techniques [9], which measure thermal fields on specimen boundaries, provide useful experimental data. Information on internal

---

sources can then be extracted from boundary thermal full-field data by solving an inverse heat source problem (IHSP) [20, 15], which is the main focus of this article.

Source identification in general is known to be ill-posed, as uniqueness and continuous dependence of data on f cannot usually be assured [20]. Source inverse problems using boundary observations require additional source modelling assumptions for identifiability, see specific examples in e.g. [15, 16, 22, 5]. Besides, the available literature on source identification is mainly devoted to equilibrium, rather than evolutive, situations. Various iterative inversion procedures have been applied to heat source identification, see e.g. [7, 4, 21]. Their main drawbacks are, as usual for this type of approach, the dependence of the result on the choice of initial guess and the high computational times entailed by repeated forward solutions. In addition, specialized strategies have been proposed in e.g. [19] (where the convex hull of a set of sources is reconstructed) and [26] (an algorithm we found, by conducting preliminary numerical experiments, to be highly sensitive to imperfect data).

The availability of dense boundary data permitted by infrared thermography suggests a recourse to another approach, based on the concept of reciprocity gap (RG) [2]. When the dual boundary quantities (here, the temperature and the heat flux) are completely known, any hidden feature (such as an unknown source, flaw or perturbation in material characteristics) is revealed by the fact that the reciprocity identity applied to the boundary data and another, arbitrarily chosen, trial state (often termed 'adjoint state') fulfilling the relevant field equations for a reference medium yields a nonzero value. RG-based methodologies for source identification have been investigated for scalar (thermal or electrostatic) equilibrium [16], wave propagation [17], and diffusion [18]. An algebraic algorithm for multiple point source identification under equilibrium conditions is proposed for two-dimensional configurations in [16]. This algorithm is appealing in that (i) it does not require multiple initial-boundary value problem (IBVP) solutions like usual optimization-based methodologies, and (ii) it includes a methodology for determining the number of hidden point sources. As it crucially relies on the use of harmonic polynomials as adjoint fields, its extension to source identification under transient conditions is not straightforward. RG-based approaches have also been developed for flaw identification [2, 6, 24] or electromagnetic inverse scattering [11].

In this article, the RG concept is applied to the transient IHSP in a manner making it amenable to the algebraic approach of [16]. The proposed treatment is thus restricted to spatially two-dimensional configurations, although it is open to generalizations to three-dimensional situations [23]. It allows to retrieve the number of distinct heat sources, their spatial locations and their energies. Numerical experiments under transient or static conditions are reported herein, bridging a gap with the mostly mathematical nature of the available literature for this particular type of problem and approach.

The paper is organized as follows. The IHSP of interest is defined in the remainder of this Section. The reciprocity gap functional (RGF) relevant for the present purposes is then presented in Section 2. Next, a time-integrated version of the RG that allows to exploit the algebraic approach initially developed for time-independent problems is proposed, together with the resulting identification algorithm, in Section 3. Finally, numerical experiments with that algorithm are reported, first for time-independent data and using an analytical solution for the synthetic data (Section 4), then for time-dependent data using numerically-computed synthetic data (Section 5), with the influence of noisy data discussed in both cases.

1.2. Formulation of the source identification problem

Let Ω be a bounded regular domain of $\mathbb{R}^p$ (where $p = 2, 3$ is the spatial dimensionality) whose boundary $\partial\Omega$ admits a well-defined unit normal vector n almost everywhere. The thermal evolution problem is then set on the space-time domain $\Omega \times [0, T]$, where T denotes the measurement duration.

To define a well-posed IBVP for the heat conduction arising from an assumed source f (referred to hereinafter as the forward problem), Equation (1) is supplemented by the boundary condition

$$\alpha\vartheta + k\partial_n\vartheta = \alpha\vartheta_{\text{ext}} \qquad \text{on } \partial\Omega \times [0, T] \tag{2}$$

modelling heat transfer with the external environment (with ϑ_{ext} the external temperature field, assumed uniform and constant, and α the heat transfer coefficient), and the initial condition

$$\vartheta(\cdot, 0) = \vartheta_{\text{ext}} \quad \text{in } \Omega. \tag{3}$$

Introducing the change of variable $\theta = \vartheta - \vartheta_{\text{ext}}$ and setting $x = \hat{x}/\bar{x}$, $t = \hat{t}/\bar{t}$, $\theta = \hat{\theta}/\bar{\theta}$ and $f = \hat{f}/\bar{f}$ (where $\bar{\theta}$ is a nonzero reference temperature and with the characteristic length $\bar{x}$, time $\bar{t}$ and source $\bar{f}$ defined by $\bar{x} = k/\alpha$, $\bar{t} = k^3/(\rho C\alpha^2)$ and $\bar{f} = k^3/(\rho C\alpha^2\bar{\theta})$), the IBVP defined by (1), (2) and (3) is recast into the simple, non-dimensional form

$$(\partial_{\hat{t}} - \hat{\Delta})\hat{\theta} = \hat{f} \qquad\qquad \text{in } \hat{\Omega} \times [0, \hat{T}] \tag{4a}$$

$$(\partial_{\hat{n}} + 1)\hat{\theta} = 0 \qquad\qquad \text{on } \partial\hat{\Omega} \times [0, \hat{T}] \tag{4b}$$

$$\hat{\theta}(\cdot, 0) = 0 \qquad\qquad \text{in } \hat{\Omega}, \tag{4c}$$

on which the remainder of this article is based (with the non-dimensional form of all variables implicitly understood and all hat symbols hereinafter dropped to avoid cumbersome notations).

The IHSP thus consists in identifying the source distribution f from space-time boundary data θ_{m}:

$$\theta = \theta_{\text{m}} \qquad \text{on } \partial\Omega \times [0, T]. \tag{5}$$

The heat flux $\partial_n\theta$ is then also known from the data θ_{m} by virtue of the boundary condition (4b). In this article θ_{m} is assumed to be known on the whole lateral boundary $\partial\Omega \times [0, T]$. In case of data collected over time but only on a part of $\partial\Omega$, the proposed identification procedure remains conceivably applicable if preceded by a data completion step [3, 10].

1.3. Modelling assumptions for the source term

As pointed out in [20], a major difficulty is the non-identifiability of general source terms. A review of existing modelling assumptions can be found in [19]. In this article, multiple time-modulated point sources are considered, with the time modulation restricted to piecewise-constant powers. The sought sources are thus assumed to have the form

$$f(x, t) = \sum_{j=1}^{N} p_j\delta(x - s_j)\Pi\left(\frac{t - t_j}{\ell_j}\right) \tag{6}$$

where $\Pi(\cdot)$ is a normalized box function defined in terms of the Heaviside step function $\text{H}(\cdot)$ by $\Pi(t) = \text{H}\left(t + \frac{1}{2}\right) - \text{H}\left(t - \frac{1}{2}\right)$. The set of unknown sources (6) is thus characterized by the source spatial and temporal locations s_j, t_j, powers p_j and holding times ℓ_j; moreover, the total number N of sources is not known *a priori* and is thus also sought.

Additionally, the sources to be identified are assumed to be spatially well separated (i.e., $s_i \neq s_j$ for $i \neq j$) and inactive after a finite extinction time $t^\star$ (i.e. $t_j + \ell_j \leq t^\star$, $1 \leq j \leq N$). A lower threshold p_{thr} on source power will also be taken into account. Under these assumptions, Theorem 2.1 of [18] holds, i.e. sources are uniquely identifiable from the temperature and heat flux distributions on the boundary associated with one experiment.

The chosen modelling assumptions and the assumed format (5) of the available supplementary data are well suited to the extraction of information using a reciprocity gap (RG) functional. The RG-based formulation for the present heat source identification problem is now presented.

2. Reciprocity Gap Method

2.1. Formulation

Reciprocity gap functionals are set up by resorting to an adjoint field ψ, which in the present transient heat conduction setting is governed by the homogeneous heat equation with time reversed:

$$(\partial_t + \Delta)\psi = 0, \quad \text{in } \Omega \times [0, T]. \tag{7}$$

On applying the third Green's identitiy to (4a) and (7), integrating the resulting equality in time over $\tau \in [0, t]$, and using boundary condition (4b), initial condition (4c) and observation (5), one obtains:

$$\int_{\partial\Omega \times [0,t]} (\partial_n \psi + \psi) \theta_{\mathrm{m}} \, ds \, d\tau + \int_{\Omega} \theta(\cdot, t) \psi(\cdot, t) \, dv = \int_{\Omega \times [0,t]} f\psi \, dv \, d\tau. \tag{8}$$

This identity thus links information on time-varying point sources in $\Omega \times [0, t]$ with measured space-time data on $\partial\Omega \times [0, t]$. This is emphasized by symbolically reformulating it as

$$\mathcal{R}(\psi, t) = \mathcal{S}(\psi, t) \qquad \forall \psi \text{ solution of (7)}, \ \ \forall t \in [0, T], \tag{9}$$

where the source term functional $\mathcal{S}$ is defined by

$$\mathcal{S}(\psi, t) := \int_{\Omega \times [0,t]} f\psi \, dv \, d\tau \tag{10}$$

and $\mathcal{R}$ is the *reciprocity gap functional* (RGF), defined by

$$\mathcal{R}(\psi, t) := \mathcal{R}_{\mathrm{L}}(\psi, t) + \mathcal{R}_{\mathrm{B}}(\psi, t) \tag{11}$$

in terms of the "lateral" RGF $\mathcal{R}_{\mathrm{L}}$ collecting lateral (experimental) information over $\partial\Omega \times [0, t]$ and the "base" RGF $\mathcal{R}_{\mathrm{B}}$ collecting information at the final time t, with

$$\mathcal{R}_{\mathrm{L}}(\psi, t) := \int_{\partial\Omega \times [0,t]} (\partial_n \psi + \psi) \theta_{\mathrm{m}} \, ds \, d\tau, \quad \mathcal{R}_{\mathrm{B}}(\psi, t) := \int_{\Omega} \theta(\cdot, t) \psi(\cdot, t) \, dv. \tag{12}$$

The reciprocity gap equality (9) links causes hidden in Ω (featured in $\mathcal{S}$) to their measurable consequences (featured in $\mathcal{R}$). The nature of the two components $\mathcal{R}_{\mathrm{L}}$ and $\mathcal{R}_{\mathrm{B}}$ of $\mathcal{R}$ is, however, quite different, as $\mathcal{R}_{\mathrm{L}}(\psi, T)$ is observable while $\mathcal{R}_{\mathrm{B}}(\psi, T)$ is not. Following this remark, equality (9) can be considered as linking the observable quantity $\mathcal{R}_{\mathrm{L}}(\psi, t)$ to an *apparent source* functional $\mathcal{H}(\psi, t)$, through

$$\mathcal{R}_{\mathrm{L}}(\psi, t) = \mathcal{H}(\psi, t) \qquad \text{with} \quad \mathcal{H}(\psi, t) := \mathcal{S}(\psi, t) - \mathcal{R}_{\mathrm{B}}(\psi, t). \tag{13}$$

One now needs a strategy (and in particular a suitable set of adjoint test-functions $\{\psi_k\}_{k\in\mathbb{N}}$) allowing to extract information about the unknown source system. In particular, it is important to remove, or minimize, the non-observable contribution $\mathcal{R}_\mathrm{B}$ to $\mathcal{R}$. This can be done in at least two different ways:

(a) Use adjoint fields $\psi(x,\tau)$ that vanish at final time $\tau = t$ (hence $\mathcal{R}_\mathrm{B} = 0$). Such adjoint fields are available in analytical form involving Fourier-Bessel series (see Appendix A). However, their complicated expressions preclude the use of simple analytical or algebraic approaches such as those proposed for time-independent problems in previously-mentioned works on RG-based identification. Instead, iterative algorithms (e.g. root-finding methods) must be applied for extracting information from the $\mathcal{R}_\mathrm{L}(\psi, t)$.

(b) Exploit measurements made over a duration T sufficiently large to make the non-observable component $\mathcal{R}_\mathrm{B}$ negligible. This approach is followed here as it permits more flexibility in choosing adjoint fields. In particular, harmonic time-independent adjoint fields can be used (whereas they are not permitted by treatment (a)), allowing a natural extension of previously-proposed algebraic treatments. This essentially requires making measurements until much later than the extinction time $t^\star$ of the last active source (a limitation which clearly does not affect treatment (a)).

3. Reciprocity gap method in time-integrated form

3.1. The large observation time limit

Let $t^\star$ denote the extinction time of the last active source to be identified. For a fixed adjoint field ψ, the function $t \mapsto \mathcal{S}(\psi, t)$ is constant for $t > t^\star$, so that

$$\forall t > t^\star, \ \mathcal{R}_\mathrm{L}(\psi, t) = \mathcal{S}(\psi, t^\star) - \mathcal{R}_\mathrm{B}(\psi, t). \tag{14}$$

Moreover, for $t > t^\star$, the system evolves towards thermal equilibrium, and in particular (see [1], Prop. 8.4.1) one has $\lim_{t\to\infty} \theta(x, t) = 0$, which implies

$$\lim_{t\to\infty} \mathcal{R}_\mathrm{B}(\psi, t) = 0 \tag{15}$$

for any adjoint field that remains bounded as $t \to +\infty$. For an infinite observation duration, exploiting (15), one thus obtains:

$$\mathcal{R}(\psi, \infty) = \mathcal{S}(\psi, t^\star), \tag{16}$$

allowing to exploit the RG values at large times for source identification.

3.2. RG with time-independent adjoint fields

We now consider exploiting the RG equality in its limiting form (16) by using time-independent (and hence harmonic) adjoint fields ψ. Consider the time-integrated quantities

$$\Theta(x) = \int_0^\infty \theta(x, \tau)\,\mathrm{d}\tau \quad ; \quad F(x) = \int_0^\infty f(x, \tau)\,\mathrm{d}\tau \tag{17}$$

which are well-defined since all sources are assumed inactive for $t \geq t^\star$. They are readily found by directly time-integrating (4a), (4b) and invoking the initial and final conditions (4c) and (15) to satisfy the following Poisson BVP:

$$\Delta\Theta = F \quad (\text{in } \Omega), \qquad (\partial_n + 1)\Theta = 0 \quad (\text{on } \partial\Omega). \tag{18}$$

5

Then, for any harmonic adjoint field Ψ, the components of the RG equality (16) are given by:

$$\mathcal{R}(\psi,\infty) = \int_{\partial\Omega} \Theta_{\mathrm{m}}(\partial_n\Psi + \Psi)\,\mathrm{d}s, \qquad \mathcal{S}(\psi,t^\star) = \int_\Omega F\Psi\,\mathrm{d}v \tag{19}$$

where Θ_{m} is the time-integrated version of the data θ_{m}. Moreover, with the chosen source model (6), one obtains

$$\mathcal{S}(\psi,t^\star) = \sum_{j=1}^N \lambda_j\Psi(s_j) \tag{20}$$

where $\lambda_j = p_j\ell_j$ (or $\lambda_j = \int_0^\infty p_j(\tau)\,\mathrm{d}\tau$ for more general source modulations) is the energy of the j-th source.

Since integrating over an infinite observation duration has reduced the heat equation to the Poisson equation, the algebraic method introduced in [16] for exploiting the RG identity in the time-independent case can be applied. Being based on a complex-variable formulation of the adjoint fields, this approach assumes a spatially two-dimensional setting (however, [16] and [23] propose ways to extend this approach to three-dimensional configurations).

3.3. Adjoint fields

From now on, a spatially two-dimensional setting is assumed, with complex polynomials used for adjoint fields (such functions, being holomorphic, have harmonic real and imaginary parts). Associating $\mathbb{R}^2$ with $\mathbb{C}$ through $x_1 + ix_2 = z$, the following family of test functions is defined:

$$\Psi_k(x) = z^k, \quad k \in \mathbb{N}. \tag{21}$$

The components of the RG equality (16) are then given by:

$$\mathcal{R}(\Psi_k,\infty) = \int_{\partial\Omega} \Theta_{\mathrm{m}}(kn_z + z)z^{k-1}\,\mathrm{d}s =: \alpha_k, \qquad \mathcal{S}(\psi,t^\star) = \sum_{j=1}^N \lambda_j\sigma_j^k \tag{22}$$

where σ_j denotes the affix of the j-th source location s_j. The source reconstruction thus consists in finding the locations σ_j and energies λ_j verifying the RG equality (wherein the known quantities α_k are defined by (22))

$$\sum_{j=1}^N \lambda_j\sigma_j^k = \alpha_k. \tag{23}$$

3.4. Reconstruction procedure: perfect data

The algebraical method previously introduced in [16] for source identification in elliptic system is now summarized. It assumes, as *a priori* information, that an upper bound $M \geq N$ of the correct number N of unknown sources is known. For $m,n \leq M$, let the RG values $\mathcal{R}(\Psi_k,\infty)$ that synthesize available measurements be arranged into $m \times n$ complex-valued observation matrices $H^0_{m,n}$ and $H^1_{m,n}$ defined by

$$H^0_{m,n} = [\alpha_{i+j-2}]_{1\leq i\leq m,\,1\leq j\leq n} = [\mathcal{R}(\Psi_{i+j-2},\infty)]_{1\leq i\leq m,\,1\leq j\leq n}, \tag{24a}$$

$$H^1_{m,n} = [\alpha_{i+j-1}]_{1\leq i\leq m,\,1\leq j\leq n} = [\mathcal{R}(\Psi_{i+j-1},\infty)]_{1\leq i\leq m,\,1\leq j\leq n} \tag{24b}$$

The unknowns N, σ_j and λ_j can then be recovered via the following procedure:

Algorithm 1 *(reformulation of Theorem 2 of [16])*

1. *The rank of $H^0_{M,M}$ equals N, and its first N columns are linearly independent (i.e. $H^0_{M,n}$ has rank N for any $n \geq N$). This allows to determine N by evaluating the rank of $H^0_{M,M}$ (or, equivalently, of $H^0_{M,n}$ for all $n \leq M$ until a stationary rank is reached).*
2. *Once N is known, the source locations σ_j are the eigenvalues of $H^1_{N,N}(H^0_{N,N})^{-1}$.*
3. *Finally, once N and σ_j are known, the energies λ_j are found by simply solving the RG equations (23), linear in λ_j, with $0 \leq k \leq N-1$.*

Implementing this procedure requires prior evaluation of $\alpha_k = \mathcal{R}(\Psi_k, \infty)$ for $0 \leq k \leq 2M - 1$. Besides, the governing matrix $[\sigma_j^k]$ ($0 \leq k \leq N-1$, $1 \leq j \leq N$) for this last step is a Vandermonde matrix, making the estimation of λ_j potentially sensitive to rounding errors in the evaluation of $\{\alpha_k\}$.

3.5. Reconstruction procedure: noisy data

In practice, the accurate determination of N from the rank of $H^0_{M,M}$ is not easy because the trailing eigenvalues of the latter will usually be small, but nonzero, due to numerical approximations (in e.g. the evaluation of integrals defining the α_k) and rounding errors. It is suggested in [16] to define N as the smallest n such that the columns of $H^0_{M,n+1}$ verify a linear-dependence relationship within a tolerance ϵ (rather than exactly), while N is sought in [23] as the smallest n such that $\det\left(H^0_{n+1,n+1}\right) = 0$.

Those approaches are no longer suitable when noisy data is used, as is always the case with real experiments. We propose instead the following procedure for determining N from noisy data, which is a modified version of Algorithm 1 where the exact rank of $H^0_{M,M}$, expected to be equal to M rather than N, is not explicitly sought *a priori*. Instead, only sources whose energy is above a threshold λ_{thr} are retained as physically relevant (which amounts to defining and evaluating a numerical rank for $H^0_{M,M}$):

Algorithm 2

1. *Compute source locations σ_j as the eigenvalues of $H^1_{M,M}(H^0_{M,M})^{-1}$.*
2. *Find the corresponding energies λ_j by solving the RG equations*

$$\sum_{j=1}^{M} \lambda_j \sigma_j^k = \alpha_k \qquad (0 \leq k \leq M-1). \tag{25}$$

   Renumber the σ_j and λ_j so that $|\lambda_1| \geq |\lambda_2| \ldots \geq |\lambda_M|$.
3. *Evaluate the* estimated number of sources $N_{est}(M, \lambda_{thr})$ *as*

$$N_{est}(M, \lambda_{thr}) = \max\left\{j \,\middle|\, |\lambda_j| \geq \lambda_{thr}\right\}. \tag{26}$$

   Retain $(\sigma_j, \lambda_j)_{1 \leq j \leq N_{est}}$ as identified sources, discard $(\sigma_j, \lambda_j)_{j > N_{est}}$.

source #	x_1	x_2	λ_j	t_{mj}	ℓ_j	p_j
S_1	0.25	0, 5	0.04	0.025	0.05	1
S_2	-0.25	-0.25	0.06	0.125	0.05	1
S_3	0.5	0	0.04	0.225	0.05	1
S_4	-0.3	0.1	0.1	0.425	0.05	1
S_5	0.5	-0.6	0	0.425	0.05	1

Table 1: Source characteristics ($\sigma_j = x_{1,j} + \mathrm{i}x_{2,j}$); S_5 is used only in Section 5

4. Numerical experiments: time-independent data

The RG-based source identification is first illustrated on a time-independent example. The domain Ω is the disk of radius 2 centered at the origin. Four point sources $S_1, \ldots, S_4$, whose locations and energies are given in Table 1, are to be identified from time-independent temperature data Θ_{m} on $\partial\Omega$ (hence $N = 4$). The noisy-corrupted simulated temperature data is given by

$$\Theta_{\mathrm{m}} = \sum_{j=1}^{N} \lambda_j \mathcal{G}(\cdot; s_j) + \delta\mathcal{N} = \Theta_{\mathrm{m,exact}} + \delta\mathcal{N} \tag{27}$$

where $x \mapsto \mathcal{G}(\cdot; \sigma)$ is the Green's function of the Laplace's equation for a unit source located at $\sigma \in \Omega$, which is known analytically (see Appendix B) for the disk-shaped domain and boundary condition (4b) considered for this example, $\mathcal{N}$ is a white Gaussian noise whose root mean square amplitude is equal to that of $\Theta_{\mathrm{m,exact}}$, and δ is the noise level relative to the reference implicit in the definition of $\mathcal{N}$. The simulated measurement (27) is then sampled at N_Θ equally-spaced points of the circle $\partial\Omega$, and the RG values $\alpha_k = \mathcal{R}(\Psi_k)$ computed for $0 \leq k \leq 2M - 1$ using a N_Θ-point trapezoidal quadrature rule.

Estimation of the number of sources. Figure 1 shows the estimated number $N_{\mathrm{est}}(M, \lambda_{\mathrm{thr}})$ of sources for $\lambda_{\mathrm{thr}} = 2 \times 10^{-3}$ as a function of the assumed maximum number M of sources, for various noise levels δ and two measurement densities $N_\Theta = 100$ and $N_\Theta = 500$. The correct number $N = 4$ of sources is found in all cases with $M = 4$ or $M = 5$ and also for larger values of M when δ is small enough. Moreover, one notes that the larger measurement density $N_\Theta = 500$ yields, on average, a better estimate of N from noisy data.

The ability of the RG-based method to correctly identify the number of unknown sources can also be assessed by other means. Consider the distribution of the singular values h_i ($1 \leq i \leq M$) of $H^0_{M,M}$, which are plotted in Figure 2 for various measurement densities, with $M = 6$ and $M = 10$ and $\delta = 0$, 10^{-3} and 2×10^{-2}. One sees in particular that $h_i \approx 0$ ($i > N = 4$) for noise-free data ($\delta = 0$), except for the coarsest measurement density $N_\Theta = 25$ (i.e. the correct number N of sources is identified), while for noisy data the drop between h_N and h_{N+1} gets sharper as N_Θ increases and δ decreases, and also as M goes from $M = 6$ to $M = 10$ while N_Θ and δ are fixed. This is due to the fact that matrix $H^0_{M,M}$ requires the RG values α_k for $0 \leq k \leq 2M - 1$: since the traces on $\partial\Omega$ of the adjoint fields Ψ_k are increasingly oscillating functions, the effect of measurement errors on the accuracy of α_k increases with k. Finally, to assess the average effect of noise on source number estimation, 200 realizations of noisy data have been generated for each noise level δ, and the number of times (out of 200) for which the correct number of sources is identified is given in Table 2 for various values of δ and measurement density N_Θ. One sees that
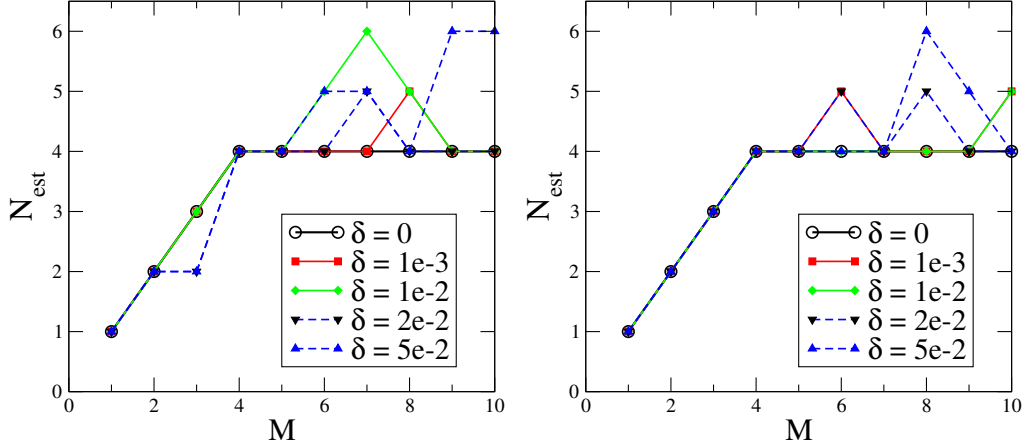
8

Figure 1: Time-independent source identification: $N_{\text{est}}(M, \lambda_{\text{thr}})$ for various noise levels δ, with $\lambda_{\text{thr}} = 2 \times 10^{-3}$ and $N_\Theta = 100$ (top) or $N_\Theta = 500$ (bottom).

N_Θ \ δ	0	10^{-4}	10^{-3}	10^{-2}	2×10^{-2}	5×10^{-2}	10^{-1}
50	200	199	185	171	163	89	55
100	200	199	184	179	173	108	81
500	200	200	190	180	177	164	119
1000	200	200	192	173	174	177	145

Table 2: Time-independent source identification, noisy data: number of noise realizations (out of 200) for which the correct number of sources is identified, for various values of the noise level δ and measurement density N_Θ.

the procedure is sensitive to noise, the correct number of sources being consistently identified only for low noise levels (less than about one percent).

Identification of the source locations and energies. Once the number of sources is known, their locations and energies are estimated. For a given number of sources this procedure can be shown to be stable. The absolute discrepancies d_{L} (in location) and d_{E} (in energy) between two sets $A = \{\sigma_j, \lambda_j\}_{1 \leq j \leq N}$ and $B = \{\sigma'_j, \lambda'_j\}_{1 \leq j \leq N}$ of sources can be quantified [5] as

$$d_{\text{L}}(A, B) = \sum_{j=1}^{N} |\sigma_j - \sigma'_{\pi(j)}|, \qquad d_{\text{E}}(A, B) = \sum_{j=1}^{N} |\lambda_j - \lambda'_{\pi(j)}| \qquad (28)$$

with the permutation π defined by $\pi := \arg\min_{\varpi \in S_N} \sum_{j=1}^{N} |\sigma_j - \sigma'_{\varpi(j)}|$. The total absolute discrepancy is measured by $d(A, B) = d_{\text{L}}(A, B) + d_{\text{E}}(A, B)$ (conventionally setting $d(A, B) = \infty$ if $N_A \neq N_B$). Moreover, the following stability result about $d(A, B)$ is given in [5]:

Theorem 1 ([5], Theorem 1.3.4) *Assume that there exist real, strictly positive constants M_1, M_2, R such that two sets A and B of sources satisfy*

$$|\sigma_j - \sigma_k| \geq M_1, \qquad |\sigma'_j - \sigma'_k| \geq M_1, \qquad |\sigma_j - \sigma'_k| \geq M_1 \qquad (j \neq k);$$
$$|\lambda_j| \geq M_2 \quad ; \qquad |\lambda'_j| \geq M_2; \qquad |z| \leq R.$$
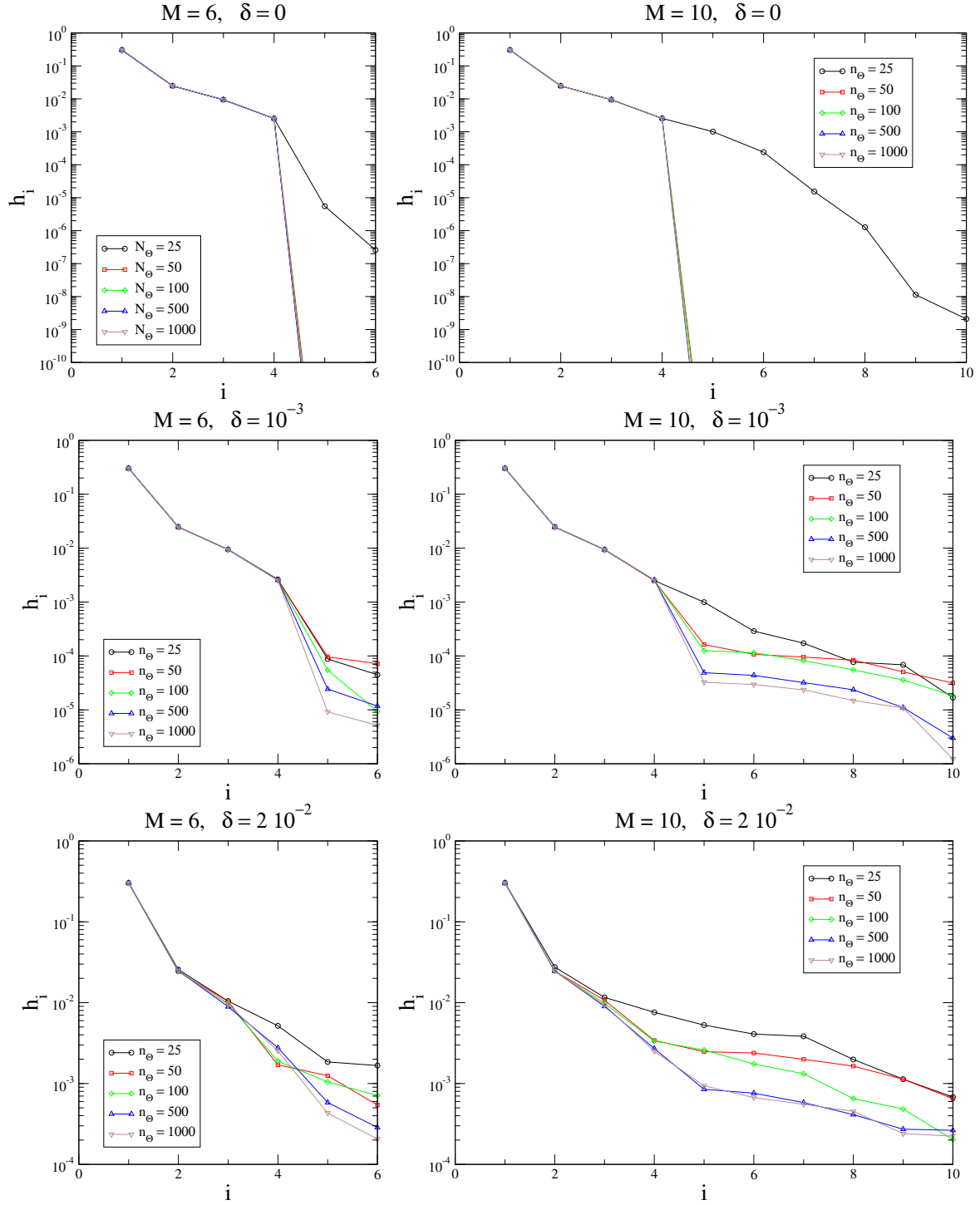
9

Figure 2: Time-independent source identification: singular values of $H_{M,M}^0$ for various measurement densities, with $M = 6$ (left) and $M = 10$ (right) and $\delta = 0$ (top), $\delta = 10^{-3}$ (middle) and $\delta = 2 \times 10^{-2}$ (bottom).

N_Θ	$\delta = 0$		$\delta = 10^{-3}$		$\delta = 10^{-2}$	
	$d_{\mathrm{L}}^{\mathrm{rel}}$	$d_{\mathrm{E}}^{\mathrm{rel}}$	$d_{\mathrm{L}}^{\mathrm{rel}}$	$d_{\mathrm{E}}^{\mathrm{rel}}$	$d_{\mathrm{L}}^{\mathrm{rel}}$	$d_{\mathrm{E}}^{\mathrm{rel}}$
100	5.1×10^{-14}	1.9×10^{-13}	1.7×10^{-02}	6.0×10^{-02}	5.5×10^{-01}	5.7×10^{-01}
500	1.4×10^{-14}	5.1×10^{-14}	7.6×10^{-03}	2.7×10^{-02}	2.4×10^{-01}	2.5×10^{-01}
1000	1.5×10^{-14}	5.6×10^{-14}	5.3×10^{-03}	1.9×10^{-02}	1.4×10^{-01}	1.7×10^{-01}

Table 3: Time-independent point source identification, noisy data: reconstruction errors for various noise levels δ and measurement densities N_Θ.

Then, the thermal boundary data $\bar\theta_A$ and $\bar\theta_B$ corresponding respectively to source sets A and B satisfy $d(A,B) \leq c(M_1, M_2, \Omega, R)\|\bar\theta_A - \bar\theta_B\|_{L^2(\partial\Omega)}$.

A local Lipschitz stability result of a similar nature is established in [14] for time-independent point source identification in anisotropic media. Moreover, source locations σ_i are found from an eigenvalue problem (step 1 of Algorithm 2), and matrix perturbation theory [13] shows that (simple) eigenvalues are continuous functions of the matrix, consistently with the above-quoted theorem. Hence, the high sensitivity to noise observed for the time-independent data means that the condition numbers (acting as sensitivity coefficients) for these eigenvalues are high.

In the following, source reconstruction errors will be conveniently quantified in terms of the relative mean discrepancies

$$d_{\mathrm{L}}^{\mathrm{rel}} = \Big(\sum_{j=1}^{N} |\sigma_j^{\mathrm{true}}|\Big)^{-1} d_{\mathrm{L}}, \qquad d_{\mathrm{E}}^{\mathrm{rel}} = \Big(\sum_{j=1}^{N} |\lambda_j^{\mathrm{true}}|\Big)^{-1} d_{\mathrm{E}}. \qquad (29)$$

For example, results for the identification of the set of time-independent sources of Table 1 are shown in Table 3, in terms of the relative discrepancies (29) averaged over 200 realizations of the simulated noise. Accurate identification using time-independent data is again seen to require very low levels of noise.

5. Numerical experiments: time-dependent case

Multiple source identification using transient thermal data is now considered, with Ω taken as the disc of unit radius centered at the origin. Five point sources $S_1, \ldots, S_5$ are defined (in terms of their spatial and temporal location, power and holding time) in Table 1. Synthetic transient data is numerically generated for three different sets of sources, namely $\mathbb{S}_1 = \{S_1, S_2, S_3\}$, $\mathbb{S}_2 = \mathbb{S}_1 \cup \{S_4\}$ and $\mathbb{S}_3 = \mathbb{S}_2 \cup \{S_5\}$, using the Comsol software environment [12]. The identification of the sets $\mathbb{S}_i$ from their respective simulated thermal data is then considered. Sets $\mathbb{S}_1$ and $\mathbb{S}_2$ are made of spatially and temporally well-separated sources, while $\mathbb{S}_3$ features two simultaneously-active sources S_4 and S_5. The computations use an approximate version of the time-modulation box function Π, resulting in a source energy $\lambda = 0.04p$.

The numerical results of this Section are based on the following parameters: observation duration $T_{\mathrm{obs}} = 4 \sim 8t^\star$, time step 5×10^{-4}, energy threshold $\lambda_{\mathrm{thr}} = 0.005$. RG evaluations again use a trapezoidal quadrature rule.

Noise-free data, point sources. The RG-based identification procedure is first assessed on noise-free simulated data for $N_\Theta = 480$ equally-spaced measurement points on $\partial\Omega$. To study the convergence of the identification procedure with increasing measurement durations, the sets of singular values
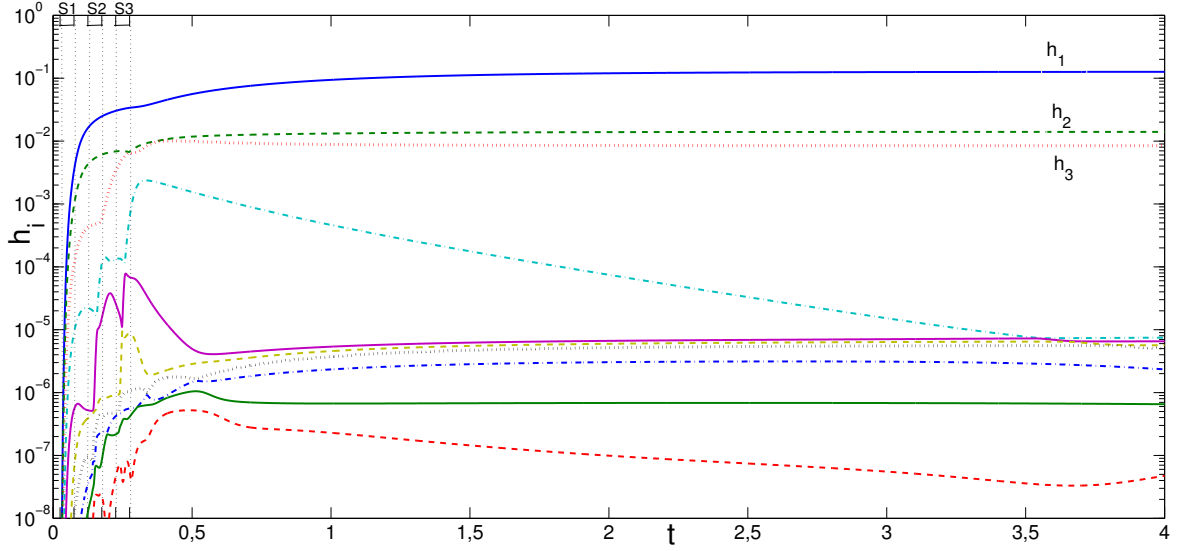
Figure 3: Transient point source identification, source set $\mathbb{S}_1$, noise-free data: evolution of singular values $h_i(t)$ of $H_{M,M}(t)$.
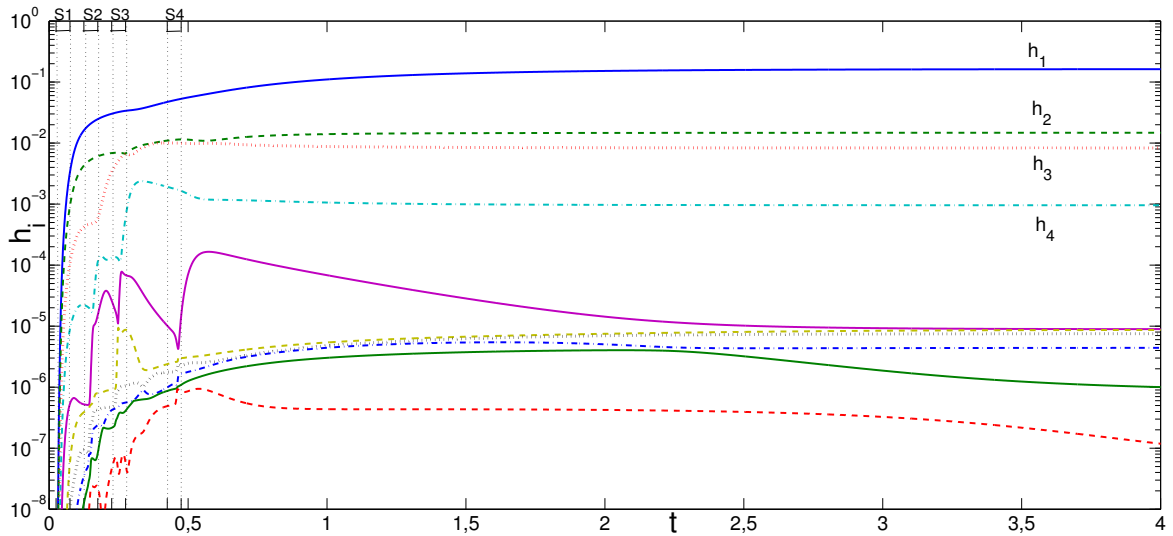

Figure 4: Transient point source identification, source set $\mathbb{S}_2$, noise-free data: evolution of singular values $h_i(t)$ of $H_{M,M}(t)$.

$h_i(t)$ of $H^0_{M,M}(t)$ are plotted against t for $t \leq T_{\text{obs}}$ in Figures 3, 4 and 5, corresponding respectively to the identification of $\mathbb{S}_1$, $\mathbb{S}_2$ and $\mathbb{S}_3$. In each case, the largest N singular values reach stabilized values for $t \approx 1$; moreover their values for $t = T_{\text{obs}}$ were found in all cases to be very close to their steady-state limit ($T = \infty$). Finally, $h_{N+1}(T_{\text{obs}}) < 10^{-2} h_N(T_{\text{obs}})$ was observed in each case, implying a correct estimation of the number of unknown sources from the transient thermal data.

Once N is determined, the source locations and energies can be found. Relative reconstruction errors for the identification of $\mathbb{S}_2$ using $N_\Theta = 480$, 960 or 1920 measurement points, given in Table 4 for $\delta = 0$, show that this step of the reconstruction is quite accurate when noise-free data is used.
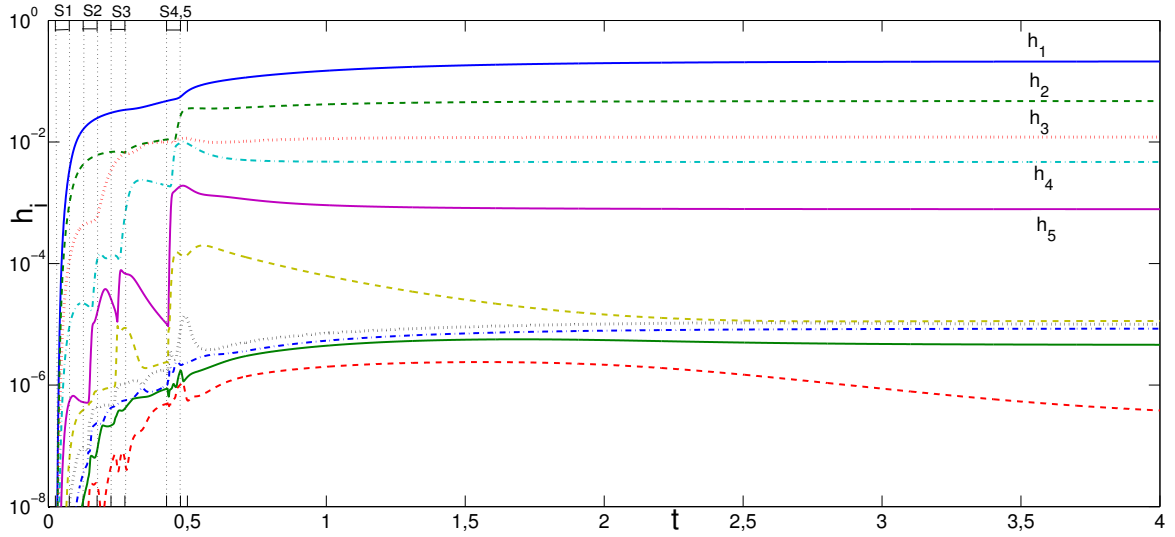
12

Figure 5: Transient point source identification, source set $\mathbb{S}_3$, noise-free data: evolution of singular values $h_i(t)$ of $H_{M,M}(t)$.

N_Θ	$\delta = 0$		$\delta = 10^{-2}$		$\delta = 10^{-1}$	
	d_L^{rel}	d_E^{rel}	d_L^{rel}	d_E^{rel}	d_L^{rel}	d_E^{rel}
480	5.3×10^{-3}	1.4×10^{-2}	1.5×10^{-2}	3.1×10^{-2}	1.5×10^{-1}	3.2×10^{-1}
960	5.2×10^{-3}	1.4×10^{-2}	1.1×10^{-2}	2.4×10^{-2}	1.0×10^{-1}	2.1×10^{-1}
1920	5.2×10^{-3}	1.4×10^{-2}	8.4×10^{-3}	1.9×10^{-2}	7.1×10^{-2}	1.4×10^{-1}

Table 4: Transient point source identification: reconstruction errors for increasing noise level δ and various measurement densities N_Θ.

Noisy data, point sources. The influence of data noise on source reconstruction is now considered, for the unknown source configuration $\mathbb{S}_2$, using again synthetic noise generated as outlined in Section 4 and with relative noise levels $\delta = 0$, 0.01 and 0.1. Overall, the obtained results show that the reconstruction from transient data is much more resistant to noise than that from steady-state data. The estimation $N_{\text{est}}(M, \lambda_{\text{thr}})$ of the number of hidden sources is correct for all noise levels considered (Figure 6), whereas the reconstruction errors for the source locations and energies remain acceptable under significant noise levels, see Table 4 where measurement densities $N_\Theta = 480$, 960 and 1920 were used. Of course, transient measurements provide much more data than steady-state measurements, and the time integration inherent in the RG functional averages out much of the noise and improves dramatically the reconstruction stability compared to the steady-state data.

Noisy data, spatially-extended sources. In this final example, the identification of sources whose support is a small disk (rather than a point) is considered in order to assess the capability of the proposed RG-based approach to identify sources whose characteristics do not correspond with the source model assumed in the identification method. Transient conditions are again assumed. The synthetic data is produced for sources $S_1, \ldots, S_5$ whose characteristics are given in Table 1, and then polluted by simulated noise using the previously-presented procedure. Reconstruction errors using $N_\Theta = 960$ and averaged over 200 realisations of the simulated noise are given in Table 5 for three cases of source support radii: (a) $r_1 = \ldots r_5 = 0.01$, (b) $r_1 = \ldots r_5 = 0.05$ and (c)
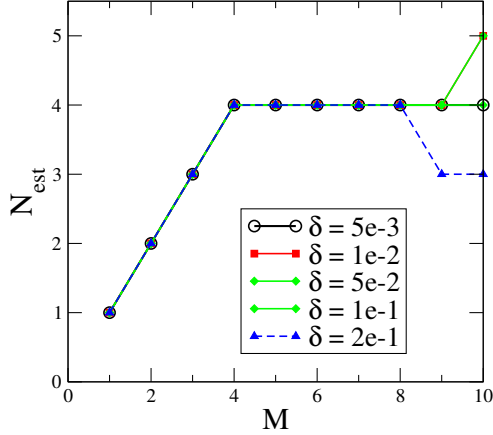
13

Figure 6: Transient point source identification, source set $\mathbb{S}_2$, noisy data: estimated number of sources $N_{\text{est}}(M, \lambda_{\text{thr}})$ for increasing relative noise levels δ ($N_\Theta = 480$).

Case	$\delta = 0$		$\delta = 10^{-2}$		$\delta = 10^{-1}$	
	$d_{\text{L}}^{\text{rel}}$	$d_{\text{E}}^{\text{rel}}$	$d_{\text{L}}^{\text{rel}}$	$d_{\text{E}}^{\text{rel}}$	$d_{\text{L}}^{\text{rel}}$	$d_{\text{E}}^{\text{rel}}$
(a)	1.1×10^{-4}	1.6×10^{-3}	3.1×10^{-2}	6.4×10^{-2}	3.3×10^{-1}	7.3×10^{-1}
(b)	1.1×10^{-4}	1.6×10^{-3}	3.2×10^{-2}	6.4×10^{-2}	3.1×10^{-1}	6.9×10^{-1}
(c)	3.5×10^{-3}	1.3×10^{-2}	2.2×10^{-2}	5.4×10^{-2}	1.9×10^{-1}	6.5×10^{-1}

Table 5: Transient extended source identification: reconstruction errors for increasing noise level δ ($N_\Theta = 960$) and $r_1 = \ldots r_5 = 0.01$ (a), $r_1 = \ldots r_5 = 0.05$ (b), $(r_1, \ldots, r_5) = (0.06, 0.03, 0.04, 0.07, 0.03)$ (c).

$(r_1, \ldots, r_5) = (0.06, 0.03, 0.04, 0.07, 0.03)$.

Discussion. The main trends emerging from these numerical experiments are as follows. For low measurement noise levels, the number, locations and energies of point sources or spatially-extended sources are accurately identified. For higher noise levels, the number of unknown sources is still correctly found while the identification accuracy deteriorates as δ increases, this degradation being more pronounced for the case of spatially-extended sources. Moreover, in most cases the source locations are more accurately reconstructed than the source energies.

6. Conclusion

In this article, a non-iterative treatment of the IHSP based on the concept of reciprocity gap is studied. Depending on how well the real source is described under the modelling assumptions for the unknown source(s) used in the proposed approach, the source estimation achieved ranges from quantitatively accurate (in which case the proposed methodology can be used on a stand-alone basis) to qualitatively reasonable (providing e.g. a suitable initial guess for a subsequent iterative refinement).

The method proposed here allows the identification of sets of spatially-localized heat sources, and more specifically to find the number of distinct heat sources, their spatial locations and their energies. The variation in time of the power of each source is not accessible. The identification method is very fast, as it does not require any numerical forward solution, unlike most iterative

14

methods [7, 4, 21]. Should more refined reconstructions (in terms of either the spatial or temporal distribution of unknown sources) be needed, this approach provides a useful initial guess for subsequent iterative inversion algorithms. Topics for future research include treating λ_{thr} as a regularization parameter to be selected algorithmically according to the noise level δ, and evaluating eigenvalue condition numbers for matrices $H^1_{M,M}(H^0_{M,M})^{-1}$ to help quantify the sensitivity to data noise of identified source locations.

The examples indicate that increasing the spatial measurement density increases the quality of the source reconstruction. From an experimental point of view, this identification approach is well suited to full-field measurement techniques such as IR thermography. The robustness of the method against measurement noise is found to be poor in time-independent conditions (SNR=46) but substantially better when transient measurements are used (SNR=20), presumably thanks to averaging effects. The next step is to test this method against experimental data, with IR thermography measurements currently being carried out at LMGC for this purpose.

Appendix A. Transient adjoint fields

Let (r,θ) denote polar coordinates in the plane. Using Fourier-Bessel series (see [25], Chap. 18), one can show that the transient adjoint field $\Psi_n(r,\theta,t)$ with vanishing initial condition $\Psi_n(r,\theta,0) = 0$ and large-time limit $\Psi_n(r,\theta,\infty) = z^n = r^n e^{\text{i}n\theta}$ is given in $D := \{r < a, 0 \leq \theta \leq 2\pi\}$ by

$$\Psi_n(r,\theta,t) = e^{\text{i}n\theta} \sum_{m\geq 1} (1 - e^{-j^2_{m,n}t}) \frac{2J_n(j_{m,n}r/a)}{j_{m,n}J_{n+1}(j_{m,n})} \tag{A.1}$$

where J_n is the Bessel function of first kind and order n, and $j_{1,n}, j_{2,n}, \ldots$ are the (real-valued, positive) zeros of J_n in order of increasing value. It can be used for any domain Ω such that $\bar{\Omega} \subset D$.

Appendix B. Point source(s) in a disk: analytical solution

The field $G(z;\sigma)$ generated by a unit point source located at $\sigma \in \mathbb{C}$ (using complex notations for points in the plane) and solving the Laplace equation in $\mathbb{C} \setminus \{\sigma\}$, i.e., the Green's function of Laplace's equation for the entire plane, is given by the well-known formula

$$G(z;\sigma) = -\frac{1}{2\pi} \text{Re} \ln(z - \sigma) \qquad z \in \mathbb{C} \setminus \{\sigma\}.$$

Considering only the case $|z| > |\sigma|$ (the other case $|z| < |\sigma|$, not needed here, being treatable by a simple adjustment of the argument to follow), $G(z;\sigma)$ can be rewritten as $G(z;\sigma) = -(2\pi)^{-1}\text{Re}[\ln z + \ln(1 - \sigma/z)]$, and the last term expanded in a convergent infinite series since $|\sigma/z| < 1$, to obtain

$$G(z;\sigma) = -\frac{1}{2\pi} \text{Re}\left\{\ln z - \sum_{n\geq 1} \frac{1}{n}(\sigma/z)^n\right\}.$$

Now, let $D_b := \{z \in \mathbb{C} \,|\, |z| < b\}$ denote the disk of radius b and C_b its boundary (i.e., the circle of radius b centered at the origin). The Green's function $\mathcal{G}(z;\sigma)$ satisfying the Robin boundary condition (4b), i.e., $\mathcal{G}(\cdot;\sigma)+\partial_n\mathcal{G}(\cdot;\sigma) = 0$ on C_b is sought. To that aim, let $\mathcal{G}(\cdot;\sigma) = G(\cdot;\sigma)+G_c(\cdot;\sigma)$, where the complementary contribution G_c is nonsingular at $z = \sigma$ and is thus sought as a power

series: $G_c(z; \sigma) = (2\pi)^{-1}\mathrm{Re}\big[\sum_{n\geq 0} \alpha_n z^n\big]$. Enforcing the Robin boundary condition at $|z| = b$, one then finds

$$\alpha_0 = \frac{1}{b} + \ln b, \qquad \alpha_n = \frac{n-b}{n(n+b)}\Big(\frac{\bar\sigma}{b^2}\Big)^n.$$

The steady-state temperature $\Theta(z)$ generated in D_b by the unit heat source located at $\sigma \in D_b$ is then given by

$$\Theta(z) = \frac{1}{2\pi b} + \frac{1}{2\pi}\sum_{n\geq 1}\frac{1}{n}\mathrm{Re}\Big[\Big(\frac{\sigma}{z}\Big)^n + \frac{n-b}{n+b}\Big(\frac{\bar\sigma z}{b^2}\Big)^n\Big].$$

The predicted boundary measurement $\Theta_{\mathrm{m}} = \Theta|_{|z|=b}$ is then obtained by setting $z = b\hat{z}$ (with $|\hat{z}| = 1$) in the above formula. Noting that $\mathrm{Re}\big(\sigma/z\big) = \mathrm{Re}\big(\bar\sigma z/b^2\big) = (\sigma\hat{\bar{z}} + \bar\sigma\hat{z})/(2b)$, one finds

$$\Theta_{\mathrm{m}}(\hat{z}; \sigma) = \frac{1}{2\pi b}\Big\{1 + \sum_{n\geq 1} b^{-n}(\sigma^n\hat{z}^{-n} + \bar\sigma^n\hat{z}^n)\Big\}. \tag{B.1}$$

The RG integrals for adjoint fields $\Psi_k = z^k$ can then easily be evaluated analytically using (B.1): since $\Psi_k = (b\hat{z})^k$ on C_b, $\mathcal{R}(\Psi_k, \infty; \sigma)$ is given by

$$\mathcal{R}(\Psi_k, \infty; \sigma) = \int_{|\hat{z}|=1}\Theta_{\mathrm{m}}(\hat{z}; \sigma)(b\hat{z})^k b\,\mathrm{d}\hat{z} = z^k$$

having used

$$\int_{|\hat{z}|=1}\hat{z}^p\,\mathrm{d}\hat{z} = 2\pi\delta_{p0} \qquad (p \in \mathbb{Z})$$

Of course, the effect of several sources σ_i with energies λ_i is obtained simply by linear combination: $\mathcal{R}(\Psi_k, \infty) = \sum_i \lambda_i \mathcal{R}(\Psi_k, \infty; \sigma_i)$.

References

[1] Allaire, G. *Numerical analysis and optimization*. Oxford (2007).

[2] Andrieux, S., Ben Abda, A. Identification of planar cracks by complete overdetermined data: inversion formulae. *Inverse Prob.*, **12**:553–563 (1996).

[3] Andrieux, S., Ben Abda, A., Baranger, T. N. Data completion via an energy error functional. *Comptes Rendus Mécanique*, **333**:171–177 (2005).

[4] Baumeister, J., Leitao, A. On iterative methods for solving ill-posed problems modeled by partial differential equations. *J. Inv. Ill-Posed Prob.*, **9**:13–29 (2001).

[5] Mdimagh, R. Identification d'inclusions de petites tailles par des méthodes quasi-explicites. Doctoral thesis, ENIT, Tunis (Tunisia) (2009).

[6] Bui, H. D., Constantinescu, A., Maigre, H. Numerical identification of linear cracks in 2D elastodynamics using the instantaneous reciprocity gap. *Inverse Prob.*, **20**:993–1001 (2004).

[7] Capatina, A., Stavre, R. Algorithms and convergence results for an inverse problem in heat propagation. *Int. J. Eng. Sc.*, **38**:575–587 (2000).

[8] Chrysochoos, A. Infrared thermography, a potential tool for analysing the material behaviour (in French). *Mécanique et Industries*, **3**:3–14 (2002).

[9] Chrysochoos, A., Belmahjoub, F. Thermographic analysis of thermo-mechanical couplings. *Arch. Mech.*, **44**:55–68 (1992).

[10] Cimetière, A., Delvare, F., Jaoua, F., Pons, F. Solution of the Cauchy problem using iterated Tikhonov regularization. *Inverse Prob.*, **17**:553–570 (2001).

[11] Colton, D., Haddar, H. An application of the reciprocity gap functional to inverse scattering theory. *Inverse Prob.*, **21**:383–398 (2005).

[12] Comsol Multiphysics. http://www.comsol.com/ (1998-2012).

[13] Demmel, J. W. *Applied numerical linear algebra.* SIAM (2007).

[14] El Badia, A. Inverse source problem in an anisotropic medium by boundary measurements. *Inverse Prob.*, **21**:1487–1506 (2005).

[15] El Badia, A., Ha Duong, T. Some remarks on the problem of source identification from boundary measurements. *Inverse Prob.*, **14**:883–891 (1998).

[16] El Badia, A., Ha Duong, T. An inverse source problem in potential analysis. *Inverse Prob.*, **16**:651–663 (2000).

[17] El Badia, A., Ha Duong, T. Determination of point wave sources by boundary measurements. *Inverse Prob.*, **17**:1127–1139 (2001).

[18] El Badia, A., Ha Duong, T. On an inverse source problem for the heat equation. Application to a pollution detection problem. *J. Inv. Ill-Posed Prob.*, **10**:585–599 (2002).

[19] Ikehata, M. An inverse source problem for heat equation and the enclosure method. *Inverse Prob.*, **23**:183:202 (2007).

[20] Isakov, V. *Inverse source problems.* American Mathematical Society (1989).

[21] Johansson, B., Lesnic, D. A procedure for determining a spacewise dependent heat source and the initial temperature. *Applic. Anal.*, **87**:265–276 (2008).

[22] Kang, H., Lee, H. Identification of simple poles via boundary measurements and an application of EIT. *Inverse Prob.*, **20**:1853–1863 (2004).

[23] Nara, T., Ando, S. A projective method for an inverse source problem of the Poisson equation. *Inverse Prob.*, **19**:355–369 (2003).

[24] Shifrin, E.I., Shushpannikov, P.S. Identification of a spheroidal defect in an elastic solid using a reciprocity gap functional. *Inverse Prob.*, **26**:055001 (2010).

[25] Watson, G. N. *A treatise on the theory of Bessel functions.* Cambridge University Press (1944).

[26] Yamatani, K., Ohnaka, K. An estimation method for point sources of multidimensional diffusion equation. *Appl. Math. Modelling*, **21**:77–84 (1997).